PHYSICAL REVIEW MATERIALS **4**, 054401 (2020)

Magnetism trends in doped Ce-Cu intermetallics in the vicinity of quantum criticality: Realistic Kondo lattice models based on dynamical mean-field theory

Munehisa Matsumoto
Institute for Solid State Physics, University of Tokyo, Kashiwa 277-8581, Japan
and Institute of Materials Structure Science, High Energy Accelerator Research Organization, 1-1 Oho, Tsukuba, Ibaraki 305-0801, Japan

(Received 30 April 2019; revised manuscript received 8 March 2020; accepted 8 April 2020; published 4 May 2020)

The quantum critical point (QCP) in the archetypical heavy-fermion compound $CeCu_6$ doped by Au is described, accounting for the localized $4f$ electron of Ce, using realistic electronic structure calculations combined with dynamical mean-field theory. Magnetism trends in $Ce(Cu_{1-\epsilon}Au_{\epsilon})_6$ ($0 < \epsilon \ll 1$) are compared with those in Co-doped $CeCu_5$, which resides on the nonferromagnetic side of the composition space of one of the earliest rare-earth permanent magnet compounds, $Ce(Co, Cu)_5$. The construction of a realistic Doniach phase diagram shows that the system crosses over a magnetic quantum critical point in the Kondo lattice in $0.2 < x < 0.4$ of $Ce(Cu_{1-x}Co_x)_5$. Comparison between Au-doped $CeCu_6$ and Co-doped $CeCu_5$ reveals that the swept region in the vicinity of QCP for the latter thoroughly covers that of the former. The implications of these trends on the coercivity of the bulk rare-earth permanent magnets are discussed.

DOI: 10.1103/PhysRevMaterials.4.054401

I. INTRODUCTION

While heavy-fermion (HF) materials and rare earth permanent magnets (REPMs) have gone through contemporary developments since the 1960s [1–9], apparently little overlap has been identified between the two classes of materials. One of the obvious reasons for the absence of mutual interest lies in the difference in the scope of the working temperatures: HF materials typically concern low-temperature physics of the order of 10 K or even lower while REPMs concern room temperature at 300 K or higher. The other reason is that the interesting regions in the magnetic phase diagram sit on opposite sides, where HF behavior appears around a region where magnetism disappears [6], while with REPMs the obvious interest lies in the middle of a ferromagnetic phase. In retrospect, several common threads in the developments for HF compounds and REPMs can be seen: one of the earliest REPMs was $Ce(Co, Cu)_5$ [4], where Cu was added to $CeCo_5$ to implement coercivity, and $CeCu_5$ was eventually identified as an antiferromagnetic Kondo lattice [10,11].

One of the representative HF compounds is $CeCu_6$ [12,13] that was discovered almost at the same time as the champion magnet compound $Nd_2Fe_{14}B$ [8,9,14]. While REPMs make up a significant part of the most important materials in the upcoming decades for a sustainable solution of the energy problem with their utility in traction motors of (hybrid) electric vehicles and power generators, HF materials might remain mostly of academic interest. But we note that a good permanent magnet is made of a ferromagnetic main-phase and less ferromagnetic subphases. For the latter compounds in REPMs, we discuss possible common physics with HF materials, namely, magnetic quantum criticality where magnetism disappears and associated scales in space-time fluctuations diverge, and propose one of the possible solutions for a practical problem on how to implement coercivity, which measures robustness of the metastable state with magnetization against externally applied magnetic fields.

Even though the mechanism of bulk coercivity on the macroscopic scale in REPMs is not entirely understood, the overall multiple-scale structure has been clear in that the intrinsic properties of materials on the microscopic scale of $O(1)$ nm is carried over to the macroscopic scale via the mesoscopic scale. Namely, possible scenarios in coercivity of Nd-Fe-B magnets [15,16] and Sm-Co magnets [17] have been so far discussed as follows.

a. Nd-Fe-B magnets. Propagating domain walls around a nucleation center of reversed magnetization are blocked before going too far. Infiltrated elemental Nd in the grain-boundary region that is paramagnetic in the typical operation temperature range of $O(100)$ K neutralizes intergranular magnetic couplings among $Nd_2Fe_{14}B$ grains [18]. Single-phase $Nd_2Fe_{14}B$ does not show coercivity at room temperature, and fabrication of an optimal microstructure on the mesoscopic scale, with the infiltrated Nd metals between $Nd_2Fe_{14}B$ grains, seems to be crucial to observe bulk coercivity.

b. Sm-Co magnets and Ce analogs. Pinning centers of domain walls are distributed over cell-boundary phases made of Sm(Co,Cu)$_5$ which separate hexagonally shaped cells of $Sm_2(Co,Fe)_{17}$. The uniformity of the cell-boundary phase [17,19] suggests that the pinning intrinsically happens on the microscopic scale in Sm(Co,Cu)$_5$ which freezes out the magnetization reversal dynamics. Also for $CeCo_5$, addition of Cu has been found to help the development of bulk coercivity [4] without much particular feature in the microstructure, suggesting here again an intrinsic origin contributing to the bulk coercivity.

Solution of the overall coercivity problem takes out-of-equilibrium statistical physics, multiscale simulations involving the morphology of the microstructure in the intermetallic materials, electronic correlation in $4f$ electrons, finite-temperature magnetism of Fe-based ferromagnets, and magnetic anisotropy, each of which by itself makes a subfield for intensive studies. Faced with such a seemingly intractable problem, it is important to build up fundamental understanding step by step. Therefore, we clarify the magnetism trends around quantum criticality in Ce-Cu intermetallics, as a part of $4f$-$3d$ intermetallics that belong to a common thread between HF materials and REPMs, in order to pinpoint a possible intrinsic contribution to the coercivity, specifically via exponentially growing length scales in spatial correlation and characteristic time in the dynamics.

The magnetization in REPMs derives from $3d$-electron ferromagnetism coming from Fe-group elements and $4f$ electrons in rare-earth elements provide the uniaxial magnetic anisotropy for the intrinsic origin of coercivity. Subphases are preferably free from ferromagnetism to help coercivity, e.g., by stopping the propagation of domain walls. In the practical fabrication of REPMs, both the main-phase compound and the other compounds for subphases should come out of a pool of the given set of ingredient elements. Investigations on nonferromagnetic materials that appear in the same composition space as the ferromagnetic material are of crucial importance for contributing the intrinsic information into the solution of the coercivity problem.

Thus we investigate the Cu-rich side of the composition space in Ce(Co, Cu)$_5$ and inspect the magnetism trends around the HF compound CeCu$_5$. It is found that Co doping into CeCu$_5$ drives the material toward a magnetic quantum critical point (QCP), to the extent that $3d$-electron ferromagnetism coming from Co does not dominate, which seems to be the case experimentally [20] when the concentration of Co is below 40%. It has also been known that Au-doped CeCu$_6$ goes into quantum criticality [21,22], a trend which is reproduced in the same simulation framework. With CeCu$_6$ as one of the most representative HF materials, experimental measurements and theoretical developments [23–25] have been extensively done. Our finding basically reproduces what has already been agreed on the location of the magnetic QCP, but the spirit of our microscopic description may not entirely be the same as some of the past theoretical works [23–25]. Our description should be more consistent with even older works [26] in the fundamental spirit with the proper incorporation of realistic energy scales based on electronic structure calculations. We may fail in catching some subtlety specific to Au-doped CeCu$_6$, but our approach should be suited rather for general purposes in providing an overview over intrinsic magnetism of f-d intermetallics to extract the common physics therein.

We set up a realistic Kondo lattice model [27,28] for these cases and see the following: (1) CeCu$_6$ sits very close to the QCP, (2) Au-induced QCPs can also be described on the basis of a conventional Kondo lattice model as downfolded from realistic electronic structure data featuring localized $4f$ electrons, at least concerning the relative location of the QCP, without invoking valence fluctuations [29] or the specialized Kondo-Heisenberg model to describe local quantum criticality [23–25], in contrast to some of those previous developments [23,24,29] for Au-doped CeCu$_6$, and (3) Co doping in CeCu$_5$ drives the material toward the QCP in the opposite direction as Au doping does in CeCu$_6$. The main results are summarized in Fig. 1, where the Au-doped CeCu$_6$ and Co-doped CeCu$_5$ are located around a magnetic QCP following a rescaled realistic Doniach phase diagram [6,27,28].

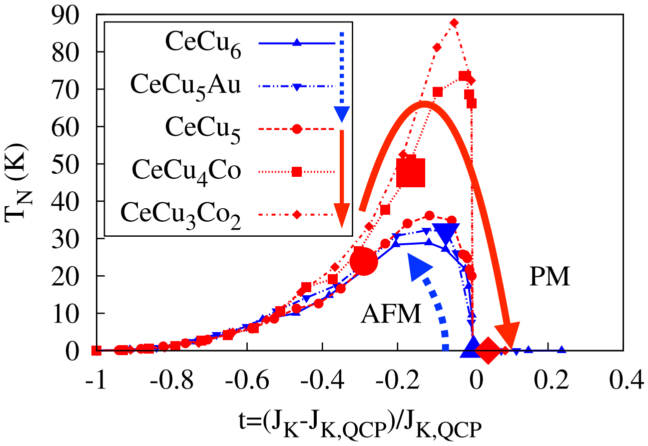

FIG. 1. Realistic Doniach phase diagram for the target compounds with a rescaled horizontal axis to measure an effective distance to the magnetic quantum critical point for each target compound. There are the antiferromagnetic (AFM) phase and the Kondo-screened paramagnetic (PM) phase. It is seen that Co-doped CeCu$_5$ moves from the magnetic side towards the Kondo-screened phase crossing the QCP, while Au-doped CeCu$_6$ moves in the opposite direction. Arrows are a guide for the eye.

The rest of the paper is organized as follows. In the next section we describe our methods [27,28] as specifically applied to the target materials: pristine CeCu$_6$, CeCu$_5$, and doped cases. In Sec. III magnetism trends in the target materials are clarified. In Sec. IV several issues remaining in the present descriptions and possible implications from HF physics on the intrinsic part of the solution of the coercivity problem of REPMs are discussed. The final section is devoted to the conclusions and outlook.

II. METHODS AND TARGET MATERIALS

We combine *ab initio* electronic structure calculations on the basis of the full-potential linear muffin-tin orbital method [30,31] and dynamical mean-field theory (DMFT) for a Kondo lattice model with well-localized $4f$ electrons [32–34], to construct a Doniach phase diagram [6] adapted for a given target material to identify an effective distance of the material to a magnetic quantum critical point. Electronic structure calculations follow density functional theory (DFT) [35,36] within the local density approximation (LDA) [36,37]. Our realistic simulation framework can be regarded as a simplified approach inspired by LDA + DMFT [38,39], where electronic structure calculations describing the relatively high-energy scales and a solution of the embedded impurity problem in the lowermost energy scales are bridged: here a realistic Kondo lattice model is downfolded [40] from the electronic structure calculations for Ce-based compounds with well localized $4f$ electrons [27,28].

More specifically, our computational framework is made of the following two steps:

(1) For a given target material, LDA + Hubbard-I [39,41] is done to extract hybridization between localized $4f$ electrons and conduction electrons, $-\mathrm{Im}\Delta(\omega)/\pi$ as a function of energy $\hbar\omega$ around the Fermi level. Position of the local $4f$-electron level below the Fermi level is determined as well.

(2) A realistic Kondo lattice model (KLM) with the Kondo coupling J_{K} is defined following the relations [27]

$$J_{\mathrm{K}} = |V|^2\left[\frac{1}{|\epsilon_f|} + \frac{1}{(\epsilon_f + U_{ff} - J_{\mathrm{Hund}})}\right], \quad (1)$$

$$|V|^2 \equiv -\frac{1}{\pi}\int_{-\infty}^{D} d\,\omega \frac{\mathrm{Tr}\Im\Delta(\omega)}{N_{\mathrm{F}}}, \quad (2)$$

which is a realistic adaptation of the Schrieffer-Wolff transformation [42] to map the Anderson model [26] to the Kondo model. Here U_{ff} and J_{Hund} are the Coulomb repulsion energy and an effective Hund coupling between $4f$ electrons, respectively, in $(4f)^2$ configuration and D is an energy cutoff [27,40] that defines the working energy window for the realistic Schrieffer-Wolff transformation. The trace in Eq. (2) is taken over all $4f$ orbitals and dividing the traced hybridization by $N_{\mathrm{F}} \equiv 14$ gives the strength of hybridization per each orbital. Experimental information on the local level splittings is incorporated for the $4f$-electron part. The thus-defined KLM is solved within DMFT using the continuous-time quantum Monte Carlo impurity solver [32]. A Doniach phase diagram [6] separating the magnetic phase and paramagnetic phase is constructed for each of the target materials and the magnetic QCP is located.

The realistic model parameters that appear in Eqs. (1) and (2) are taken on an empirical basis referring to past works [39,43], among which the origin of the on-site Coulomb repulsion energy $U_{ff} = 5\,\mathrm{eV}$ between $4f$ electrons can be traced partly back to past electronic structure calculations [44] and analyses of photoemission spectroscopy data [45]. Even though one can argue for material-specific data of U_{ff}, here we are more concerned with relative trends among the target materials within a realistic model with fixed parameters to get an overview over a group of Ce-based compounds with well-localized $4f$ electrons, rather than pursuing preciseness of each material-specific data point.

Below we describe the details of the overall procedure one by one, taking $\mathrm{CeCu_6}$ as a representative case, partly introducing the results.

A. LDA + Hubbard-I

The overall initial input here is the experimental lattice structure. This is taken from the past experimental literature for pristine $\mathrm{CeCu_6}$ in Ref. [46] and $\mathrm{CeCu_5}$ in Ref. [20], and also for $\mathrm{CeCu_5Au}$ in Ref. [47] together with the particular site preference of the dopant atom, Au. Our input lattice constants are summarized in Table I. We note that $\mathrm{CeCu_6}$ undergoes a structural phase transition between a high-temperature orthorhombic phase [46] and a low-temperature monoclinic phase [48], while $\mathrm{CeCu_5Au}$ does not [49]. In order to compare $\mathrm{CeCu_6}$ and $\mathrm{CeCu_5Au}$ on an equal footing and inspect the relative trends between them and observing that the lattice distortion introduced by the structure transition seems to be minor [49], we fix the working lattice structure of $\mathrm{CeCu_6}$ to be the orthorhombic phase and proceed to the downfolding to the realistic Kondo lattice model. The internal coordinates of atoms in $\mathrm{CeCu_6}$ and $\mathrm{CeCu_5Au}$ are shown in Table II.

For Co-doped $\mathrm{CeCu_5}$, various things happen in real experiments starting with the introduction of a ferromagnetic conduction band coming from Co and lattice shrinkage even before reaching the valence transition on the Co-rich side. Here in order to simplify the problem and to focus on the magnetism trends concerning the $4f$-electron QCP, we fix the working lattice to be that of pristine $\mathrm{CeCu_5}$ and inspect the effects of replacements of Cu by Co. Following the site preference of Co for the Cu($3g$) site as suggested in Ref. [50] for Cu-substituted $\mathrm{YCo_5}$, which we also confirm in separate calculations [51], we replace Cu by Co in the $3g$ sublattice one by one as shown in Table III for $\mathrm{CeCu_4Co}$ and $\mathrm{CeCu_3Co_2}$. With this particular setup, the effects of Co doping on $\mathrm{CeCu_5}$ have been effectively softened in our calculations. However, we will see that Co doping on $\mathrm{CeCu_5}$ drives the material

TABLE I. Inputs to LDA+Hubbard-I: the lattice constants of each target compound.

Compound	a (a.u.)	b/a (a.u.)	c/a (a.u.)	Ref.
$\mathrm{CeCu_6}$	15.3295	0.62894	1.25271	[46]
$\mathrm{CeCu_5Au}$	15.5902	0.61624	1.25576	[47]
$\mathrm{CeCu_5}$	9.702	1	0.79957	[20]
$\mathrm{CeCu_4Co}$	(fixed to be the same as $\mathrm{CeCu_5}$)			
$\mathrm{CeCu_3Co_2}$	(fixed to be the same as $\mathrm{CeCu_5}$)			

TABLE II. Inputs to LDA+Hubbard-I: internal coordinates of atoms in the orthorhombic (space group no. 62) unit cell of (a) $\mathrm{CeCu_6}$ and (b) $\mathrm{CeCu_5Au}$. The spatial translation vectors are plainly (1, 0, 0), (0, 1, 0), and (0, 0, 1), measured with respect to the lattice constants as the unit length. Each atom in the unit cell has been specified with the Wyckoff position and the internal coordinate. The input data are taken from (a) Ref. [46] and (b) Ref. [47]. It is to be noted that all of the atoms in each designated Wyckoff position contribute four atoms to the unit cell that is made of four formula units, except for Cu(1), which contributes eight atoms to the unit cell. Au has been selectively put into the Cu(2) site [47].

(a) $\mathrm{CeCu_6}$

Atom	Wyckoff	Internal coordinate
Ce	$4c$	(0.2602, 0.2500, 0.4354)
Cu(1)	$8d$	(0.4354, 0.0041, 0.1908)
Cu(2)	$4c$	(0.1467, 0.2500, 0.1418)
Cu(3)	$4c$	(0.1821, 0.7500, 0.2451)
Cu(4)	$4c$	(0.4380, 0.7500, 0.4023)
Cu(5)	$4c$	(0.0987, 0.7500, 0.4846)

(b) $\mathrm{CeCu_5Au}$

Atom	Wyckoff	Internal coordinate
Ce	$4c$	(0.26078, 0.2500, 0.43593)
Cu(1)	$8d$	(0.43493, 0.0013, 0.18791)
Au	$4c$	(0.14216, 0.2500, 0.13897)
Cu(3)	$4c$	(0.18475, 0.7500, 0.25071)
Cu(4)	$4c$	(0.44400, 0.7500, 0.39553)
Cu(5)	$4c$	(0.09178, 0.7500, 0.48395)

TABLE III. Inputs to LDA+Hubbard-I: internal coordinates of the atoms in the hexagonal (space group no. 191) unit cell of $CeCu_5$, $CeCu_4Co$, and $CeCu_3Co_2$. Here the spatial translation vectors are taken as $(-1/2, \sqrt{3}/2, 0)$, $(1/2, \sqrt{3}/2, 0)$, and $(0, 0, 1)$. In contrast to Table II, all of the constituent atoms in the same sublattice specified with the Wyckoff position are explicitly shown since the replacement of atoms happens for a selection of the atoms in the Cu($3g$) sublattice.

Atom	Wyckoff	Internal coordinate
Ce	$1a$	$(0, 0, 0)$
Cu	$2c$	$(1/2, 1/(2\sqrt{3}), 0)$
Cu	$2c$	$(1/2, -1/(2\sqrt{3}), 0)$
Cu	$3g$	$(1/4, -\sqrt{3}/4, 1/2)$
(Cu/Co)[a]	$3g$	$(1/4, \sqrt{3}/4, 1/2)$
(Cu/Co)[b]	$3g$	$(1/2, 0, 1/2)$

[a] Cu denotes $CeCu_5$ and $CeCu_4Co$; Co denotes $CeCu_3Co_2$.

[b] Cu denotes $CeCu_5$; Co denotes $CeCu_4Co$ and $CeCu_3Co_2$.

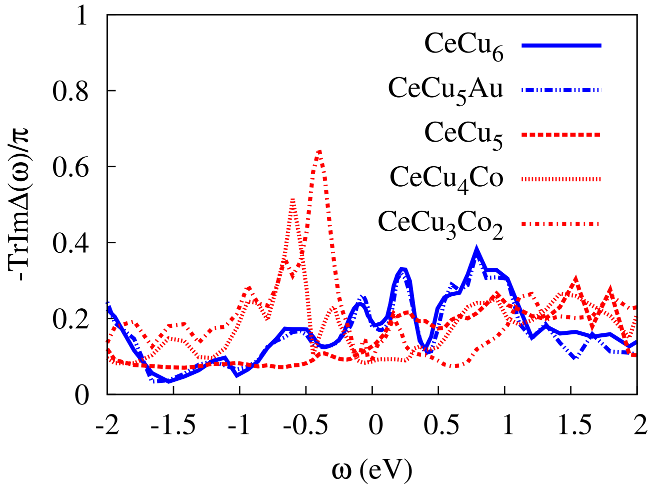

FIG. 2. Calculated hybridization function for the target compounds within LDA + Hubbard-I.

across the QCP more effectively than Au doping does for $CeCu_6$.

LDA + Hubbard-I calculations give the hybridization $-\mathrm{Im}\Delta(\omega)/\pi$ and position of the local $4f$ level, ϵ_f. The results for ϵ_f and $|V|^2$ as defined in Eq. (2) are summarized in Table IV. Raw data for $-\mathrm{Im}\Delta(\omega)/\pi$ as traced over all of the $4f$ orbitals is shown in Fig. 2.

B. DMFT for the realistic Kondo lattice model

Following Ref. [27], the hybridization function between the localized $4f$ orbital in Ce and the conduction electron band defines the material-specific KLM. Here we describe the details of the Kondo impurity problem embedded in the KLM within DMFT [52] where we use the continuous-time quantum Monte Carlo solver [53] for the Kondo impurity problem [32].

In the impurity problem embedded in DMFT we incorporate the realistic crystal-field and spin-orbit level splittings in the local $4f$ orbital of Ce. The local $4f$-electron level scheme is shown in Fig. 3. For $CeCu_6$ and hexagonal $CeCu_5$, it is known that the crystal structure splits the $j = 5/2$ multiplets into three doublets, separated by Δ_1 (meV) between the lowest doublet and the second-lowest doublet, and Δ_2 (meV) between the lowest doublet and the third-lowest doublet. Crystal-field splittings have been taken from past neutron-scattering experiments as summarized in Table V. We set the level splitting between $j = 5/2$ and $j = 7/2$ multiplets due to spin-orbit interaction to be $\Delta_{\text{spin-orbit}} = 0.3$ (eV) referring to the standard situation in Ce-based HF compounds [56].

The input obtained with LDA + Hubbard-I to our Kondo problem is shown in Fig. 2. The Kondo coupling J_{K} via a realistic variant [27] of the Schrieffer-Wolff transformation [42] is defined as in Eqs. (1) and (2). There D was the band cutoff that is set to be equal to the Coulomb repulsion $U_{ff} = 5$ (eV), and J_{Hund} is the effective Hund coupling in the f^2 multiplet to which the second term of Eq. (1) describes the virtual excitation from the $(4f)^1$ ground state.

We sweep J_{Hund} to locate the QCP on a Doniach phase diagram and also to pick up the realistic data point at $J_{\text{Hund}} = 1$ (eV). This particular choice of the Hund coupling in the virtually excited state $(4f)^2$ has been motivated [43,57] by the typical intrashell direct exchange coupling of $O(1)$ eV and an overall magnetism trend in CeM_2Si_2 (M = Au, Ag, Pd, Rh, Cu, and Ru), $CeT In_5$ (T = Co, Rh, and Ir) and pressure-induced quantum critical point in $CeRhIn_5$ as studied in our previous works, Refs. [27], [28], and [58], respectively. Thus

TABLE IV. Outputs of LDA+Hubbard-I: calculated position of localized $4f$-electron level, ϵ_f, where the offset is taken at the Fermi level, shown in the second column for each target compound. In the third column, the integrated hybridization as defined in Eq. (2) is shown.

Compound	ϵ_f (eV)	$\vert V\vert^2$
$CeCu_6$	−1.61	0.172967
$CeCu_5Au$	−1.81	0.159501
$CeCu_5$	−2.02	0.157148
$CeCu_4Co$	−1.99	0.156348
$CeCu_3Co_2$	−1.72	0.157907

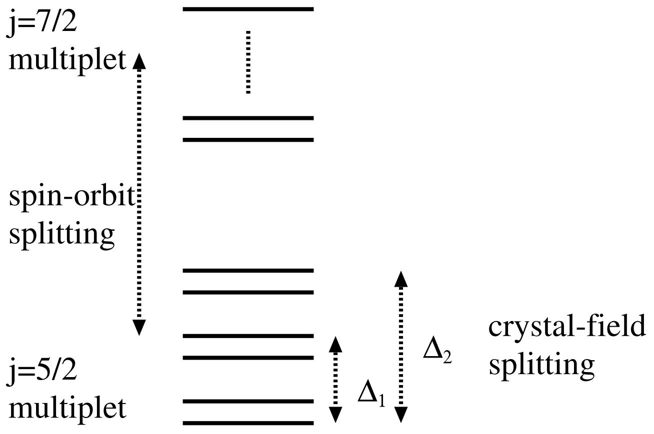

FIG. 3. Schematic picture for local-level splitting caused by spin-orbit interaction and crystal fields.

TABLE V. Input crystal-field splittings following past neutron-scattering experiments.

Compound	Crystal-field splittings	Ref.
$CeCu_6$	$\Delta_1 = 7$ meV, $\Delta_2 = 13$ meV	[54]
$CeCu_5$	$\Delta_1 \simeq \Delta_2 = 17$ meV	[55]

the working computational setup has been applied to elucidate the magnetism trends around QCP as precisely as have been done for other representative HF compounds. In practice, we define J_K at $J_{\rm Hund} = 0$ as $J_{K,0}$ and then sweep a multiplicative factor $\alpha = J_K/J_{K,0}$, calculating the temperature dependence of staggered magnetic susceptibility $\chi(\pi, T)$ for each α. In this way we can see where in the neighborhood of the QCP our target material with α corresponding to the realistic number, $J_{\rm Hund} = 1$ eV, resides on the Doniach phase diagram.

We calculate the staggered magnetic susceptibility $\chi(\pi)$ with the two-particle Green's function following the formalism developed in Ref. [34] and using a random-dispersion approximation to decouple it into single-particle Green's functions [59] which would enhance the transition temperature, in addition to the single-site mean-field nature in DMFT. The calculated data for $1/\chi(\pi)$ are shown in Fig. 4 for the case of $CeCu_6$. The temperature dependence of the reciprocal of the staggered magnetic susceptibility $1/\chi(\pi)$ is observed for each $J_K = \alpha J_{K,0}$ and we extrapolate it linearly to the low-temperature region to see if there is a finite Néel temperature. We identify that the Néel temperature vanishes in the parameter range $1.13 J_{K,0} < J_K < 1.135 J_{K,0}$, where $J_{K,0}$ is the Kondo coupling at $J_{\rm Hund} = 0$. The realistic data point is obtained by plugging in $J_{\rm Hund} = 1$ (eV) [27] and $\epsilon_f = -1.61$ (eV) (as can be found in Table IV) to Eq. (1) to be $J_K = 1.1347 J_{K,0}$. Thus the data in Fig. 4 show that $CeCu_6$ is almost right on the magnetic QCP where the Néel temperature disappears.

The same procedures are applied to all other target materials.

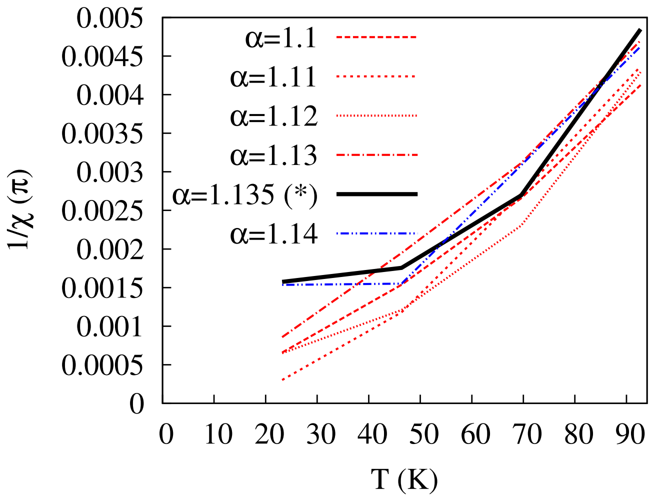

FIG. 4. Calculated temperature dependence of the reciprocal of staggered magnetic susceptibility for $CeCu_6$, the reference compound. The data with $\alpha = 1.135$, specified with an asterisk, correspond to the realistic data point.

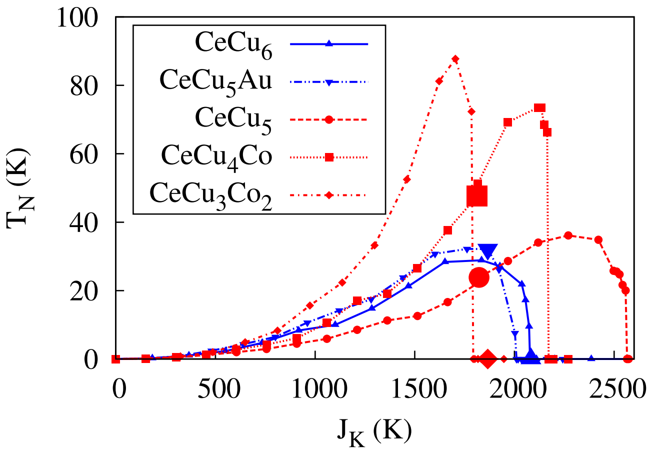

FIG. 5. Realistic Doniach phase diagram for the target compounds with the bare energy scale of the Kondo couplings.

III. RESULTS

Plotting calculated Néel temperatures with respect to $J_K = \alpha J_{K,0}$, the Doniach phase diagram is constructed for each target material as shown in Fig. 5.

By rescaling the horizontal axis of the Doniach phase diagram as follows, $t \equiv (J_K - J_{K,\rm QCP})/J_{K,\rm QCP}$ to inspect the dimensionless distance to the QCP independently of the materials [27,28], we end up with the main results as shown in Fig. 1.

A. $CeCu_6$ versus $CeCu_5$

Remarkably, $CeCu_6$ falls almost right on top of the magnetic QCP in Fig. 5. Also it is seen that the energy scales for antiferromagnetic order are on the same scale for $CeCu_6$ and $CeCu_5$ as seen in the vertical-axis scales for the calculated Néel temperatures. This may be reasonable considering the similar chemical composition between $CeCu_6$ and $CeCu_5$.

Here we note that overestimates of the calculated Néel temperature are unavoidable due to the single-site nature of DMFT and approximations involved in the estimation of two-particle Green's function [27]. Thus the calculated Néel temperature for $CeCu_5$ falling in the range of 20 K should be compared to the experimental value of 4 K [10,11] only semi-quantitatively. Nevertheless, expecting that the same degree of systematic deviations is present in all of the data for the target compounds, we can safely inspect the relative trends between $CeCu_6$ and $CeCu_5$.

B. Magnetic QCP in Au-doped $CeCu_6$

In Fig. 5 it is seen that doping Au into $CeCu_6$ only slightly shifts the energy scales competing between magnetic ordering and Kondo screening. Most importantly, Au doping drives the material towards the antiferromagnetic phase and the magnetic QCP is identified in the region $Ce(Cu_{1-\epsilon}Au_\epsilon)_6$ with $\epsilon \ll 1$, which is consistent with the experimental trends of magnetism [21,22]. This has been achieved with the control of an effective degeneracy of orbitals incorporating the realistic width of level splittings in the localized $4f$ orbital, putting the characteristic energy scales in magnetism under good numerical control in the present modeling.

While quantitative success for $\mathrm{Ce(Cu_{1-\epsilon}Au_{\epsilon})_6}$ $(0 \leqslant \epsilon \ll 1)$ concerning the location of the magnetic QCP is seen, some qualitative issues may be considered to be on the way to address magnetic quantum criticality, since this particular materials family represents the local quantum criticality scenario [23–25] where a sudden breakdown of the Kondo effect is discussed to occur on the basis of a Kondo-Heisenberg model. In our realistic model, the exchange interaction between localized $4f$ electrons naturally comes in as a second-order perturbation process with respect to the Kondo coupling [60], which is the Ruderman-Kittel-Kasuya-Yosida (RKKY) interaction [60–62].

Even though no special place for another Heisenberg term is identified in our realistic Kondo lattice model, there should indeed be other terms that are not explicitly considered. For example, with very well localized $4f$ electrons, there is another indirect exchange coupling [63] that works via the following two steps: (a) intra-atomic exchange coupling between $4f$ spin and $5d$ spin and (b) interatomic hybridization between the $5d$ band and other conduction bands. Notably, in this channel the coupling between $5d$ and $4f$ is ferromagnetic, which is in principle in competition against the antiferromagnetic Kondo coupling that we mainly consider here.

For REPM compounds such as Nd-Fe intermetallics, the latter indirect exchange coupling, which we denote J_{RT} for the convenience of reference as the effective coupling between rare-earth elements and transition metals, is dominant because $4f$ electrons are even more well localized than in Ce^{3+}-based compounds. There the Kondo couplings are not in operation practically, since f-c hybridization is weak and Kondo couplings are at too-small energy scales as compared to other exchange couplings. Now that we bring HF materials and REPM compounds on the same playground, the f-d indirect exchange couplings should also have been given more attention even though there are at the moment only some restricted prescriptions [64,66] to downfold a realistic number into J_{RT}.

This indirect exchange coupling can motivate the Heisenberg term on top of the realistic Kondo lattice model, even though it is to be noted that the sign of such extra Heisenberg terms is ferromagnetic. This may pave the way to define a realistic version of the Kondo-Heisenberg model [23–25]. Since J_{RT}'s can compete against the RKKY interaction at most only on the same order, the presence of the J_{RT} terms would not significantly alter the position of the magnetic QCP, which is brought about by the Kondo coupling that competes against the RKKY interaction as a function of the exponential of the reciprocal of the coupling constants. This way, it is hoped that there might be a way to reconcile the local QCP scenario for Au-doped $\mathrm{CeCu_6}$ and the present realistic modeling for the magnetic QCP focusing on the characteristic energy scales involving the Kondo effect.

Recent time-resolved measurements and theoretical analyses based on DMFT [67,68] for Ce(Cu,Au)$_6$ also provide a way to reconcile the local QCP scenario and experimentally detected signals from the possible Kondo quasiparticles on the real-time axis within the noncrossing approximation (NCA) [69,70] as the impurity solver in DMFT. Since our DMFT results are based on quantum Monte Carlo (QMC) methods formulated on the imaginary-time axis, migrating to the real-time data via analytic continuation poses a challenging problem [71,72], while the solution of the quantum many-body problem is numerically exact with QMC. Thus the location of the QCP derived from static observables would be better addressed with the present framework.

Still our numerically exact solution is limited to the imaginary-time direction and effects of the real-space fluctuations are not incorporated in the single-site DMFT. Recently, theoretical comparison between an exact solution of the lattice problem and DMFT has been done [73] and an artifact of DMFT to overestimate the region of antiferromagnetic phase has been demonstrated. In this respect, the present location of the magnetic QCP right below $\mathrm{CeCu_6}$ should also reflect the same artifact: if the spatial fluctuations are properly accounted for, the magnetic phase would shrink and the position of $\mathrm{CeCu_6}$ would shift slightly toward the paramagnetic side.

C. QCP to which $\mathrm{CeCu_5}$ is driven by Co doping

Co doping in $\mathrm{CeCu_5}$ shifts the energy scales more strongly than seen in Au-doped $\mathrm{CeCu_6}$. It is seen in Fig. 5 that the QCP is driven toward the smaller J_{K} side, reflecting the underlying physics in that the Kondo-screening energy scale is enhanced as Co replaces Cu. The origin of the enhanced Kondo screening is seen in Fig. 2, where anomalous peaks below the Fermi level are coming in, which should come from the almost ferromagnetic conduction band which grows into the ferromagnetism in the Co-rich side of the composition space in Ce(Cu,Co)$_5$. With 40% of Co, the $4f$-electron QCP is already passed and $\mathrm{CeCu_3Co_2}$ resides in the Kondo-screened phase. Thus it is found that the magnetic QCP of $\mathrm{Ce(Cu_{1-x}Co_x)_5}$ is located in $0.2 < x_{\mathrm{c}} < 0.4$. We note that the crystal structure and crystal-field splitting have been fixed to be that of the host material, $\mathrm{CeCu_5}$. In reality, the QCP may be encountered with smaller Co concentration.

In the present simulations, we have neglected the possible ferromagnetism in the ground state contributed by the $3d$ electrons in Co. Referring to the past experiments for Ce(Cu,Co)$_5$ described in Ref. [20], the absence of the observed Curie temperatures for the Cu-rich side with the concentration of Cu beyond 60% in the low-temperature region seems to be consistent with our computational setup in the present simulations. Even though other past work [74] for an analogous materials family Sm(Co,Cu)$_5$ does show a residual Curie temperature in the Cu-rich region, it should be noted that there is a qualitative difference in the nature of the conduction band of Cu-rich materials for the Sm and Ce-based families.

D. Universal and contrasting trends

Co-doped $\mathrm{CeCu_5}$ and Au-doped $\mathrm{CeCu_6}$ represent the different mechanisms where Co enhances f-d hybridization with the $3d$-electron magnetic fluctuations in the conduction electrons, while Au rather weakens f-d hybridization, being without d-electron magnetic fluctuations.

The trend in magnetism comes from the relative strength of exchange coupling between localized $4f$ electrons and delocalized conduction electrons. Among Ce-based intermetallic compounds, a general trend in the hybridization Δ is seen to be like the following:

$$J_K(\text{Ce-Au}) < J_K(\text{Ce-Cu}) < J_K(\text{Ce-Co}), \tag{3}$$

as is partly seen in Ref. [75] for another materials family CeT_2Si_2 (T=transition metals)—somewhere in the sequence of the trend written schematically in Eq. (3), a magnetic quantum critical point between antiferromagnetism located on the relative left-hand side and paramagnetism located on the relative right-hand side is encountered within the range where $3d$-electron ferromagnetism from Co does not dominate. The overall one-way trend from antiferromagnetism on the left-most side to paramagnetism on the right-most side in Eq. (3) is universal around the magnetic quantum criticality, while the contrasting trend between the Au-doped case and the Co-doped case in Ce-Cu intermetallics is seen from the position of the Ce-Cu intermetallics concerning the directions toward which the dopant elements drive.

The opposing trends coming from $3d$-metal dopant and $5d$-metal dopant might help in implementing a fine-tuning of the material in a desired proximity to the QCP in a possible materials design for REPMs as discussed below in Sec. IV B.

IV. DISCUSSIONS

A. Validity range of the Kondo lattice model

While we have defined the Kondo lattice model referring to the electronic structure of the target materials, the limitations on the validity range of such a downfolding approach [27,40] should be kept in mind in assessing the implications of the present results. In Sec. III B, we have already discussed the possible relation of our model to the Kondo-Heisenberg model that has been extensively used in the local QCP scenario [23–25] for $Ce(Cu_{1-\epsilon}Au_\epsilon)_6$. In a wider context, the spirit of the so-called s-d exchange model that was originally introduced by Vonsovskii [76] and Zener [77] in the early days of the theory of ferromagnetism is still alive in the indirect exchange coupling J_{RT}. This has been dropped in the present modeling for Ce-based compounds. Here we have assumed that the localization of the $4f$ electron in our Ce^{3+}-based compounds is good enough to ensure the applicability of the Kondo lattice model; at the same time, it is presumed that our $4f$ electrons in Ce^{3+}-based f-d intermetallics are not so well localized as in the case of Pr^{3+}- or Nd^{3+}-based f-d intermetallics. This means that the Kondo coupling coming from f-c hybridization would dominate over the J_{RT}'s coming from the indirect exchange coupling [63]. Such subtle interplay between different exchange mechanisms can depend on the material. Since we did not address J_{RT} in the present studies, the outcome of the possibly competing exchange interactions is not included in the present scope. Possible subtle aspects coming from the local QCP scenario might reside in this particular leftover region. If one would further opt for an alternative scenario [78], it may be useful to further investigate the effect of these dropped terms, and include them through improved algorithms based on better intuition. Although a completely *ab initio* description is desirable, to make the problem tractable we are forced into making some approximations. Here it is at least postulated that the validity of the relative location of magnetic QCP can be ensured in the present description because we have put the most sensitive coupling channel, Kondo physics, under good numerical control.

A few more discussions on the validity range of the Kondo lattice model and possible extensions are in order.

1. Toward more unbiased downfolding

The terms in our low-energy effective models have been defined by targeting the particular physics, namely, the RKKY interaction and Kondo physics. While this strategy has been good enough to address the relative trends among the target materials around the magnetic QCP, it may well have happened that other relevant terms have been dropped that do not significantly affect the location of QCP. In this regard it may be preferred either (a) to downfold from the realistic electronic structure to the low-energy effective models in a more unbiased way, at least proposing all possible candidate terms and eliminating some of them only in the final stage according to a transparent criterion, e.g., referring to the relevant energy window or (b) to work on the observables directly from first principles without downfolding. While approach (b) does not look very feasible, approach (a) might pose a feasibly challenging problem with possible help from machine learning [79] in systematically classifying the candidate terms even for such materials with multiple sublattices, multiple orbitals, and a relatively large number of orbital degeneracies as imposed from d electrons and f electrons.

2. Effects of valence fluctuations

Valence fluctuations have not been entirely incorporated in the present description of Ce compounds. Other scenarios for Au-doped $CeCu_6$ that emphasize the relevance of valence fluctuations were recently discussed [29]. We have described at least the magnetism trends around the QCP in $CeCu_6$ and $CeCu_5Au$ only with localized $4f$ electrons. Apparently valence fluctuations may not be dominant at least for magnetism. We can restore the charge degrees of freedom for $4f$ electrons and run an analogous set of simulations for a realistic Anderson lattice model in order to see any qualitative difference comes up on top of the localized $4f$-electron physics. Often the typical valence states for Ce, Ce^{4+} or Ce^{3+}, are not so clearly distinguished: even in the present Kondo lattice description, the $(4f)^0$ state with Ce^{4+} is virtually involved in the Kondo coupling and localized $4f$ electrons even contribute to the Fermi surface [80]. To pick up a few more cases, for actinides or α-Ce, either one can discuss on the basis of localized f electrons and define the Kondo screening energy scale spanning up to 1000 K, or convincing arguments can be made also on the basis of delocalized $4f$ electrons emphasizing the major roles played by valence fluctuations. Given that it does not seem quite clear how precisely the relevance or irrelevance of valence fluctuations should be formulated for the description of magnetism trends, here we would claim only the relative simplicity of our description for a magnetic QCP in $Ce(Cu_{1-\epsilon}Au_\epsilon)_6$ ($\epsilon \ll 1$). This simplification may well come with the restricted validity range.

B. Implications on the coercivity of REPM

Observing that the magnetic QCP can be encountered in the chemical composition space of Ce(Cu,Co)$_5$, we note that slowing down of spin dynamics when the system crosses over to the QCP can be exploited in intrinsically blocking the magnetization reversal processes in REPMs to help the coercivity. Since coercivity is a macroscopic and off-equilibrium notion, it is still much under development to formulate a theoretical bridge over the gap between the microscopic equilibrium properties and macroscopic coercivity. At least with QCP, diverging length scales of fluctuations and diverging relaxation times can in principle reach the macroscopically relevant spatial and time scales to help coercivity. The range of the critical region on the temperature axis and on the composition space would depend on each specific case.

In Sm-Co magnets, even though it is clear that the cell-boundary phase intrinsically carries the coercivity [3,17,19], precise characterization of the inter-relation among the intrinsic properties, microstructure, and coercivity has been still under investigation [17,19,81]. Since Sm(Cu,Co)$_5$ can be considered a hole analog of Ce(Cu,Co)$_5$ in the lowest $j = 5/2$ multiplet of Ce^{3+}, with a quest for a QCP both for magnetism and possibly also for valence fluctuations, it may help to consider the possible role of the QCP in Sm(Cu,Co)$_5$ for the intrinsic part of the coercivity mechanism. Considering the electron-hole analogy, a possible effect from the QCP for Sm(Cu$_{1-x'}$Co$_{x'}$)$_5$ can be expected in the concentration range $x'_c \simeq 1 - x_c$ (here x_c is defined in Sec. III C) which falls in $0.8 > x'_c > 0.6$. This may be compared favorably with the experimentally discussed [3] concentration of Cu in Sm-Co magnets, where up to around 35% of Cu in the cell-boundary phase made of Sm(Co,Cu)$_5$, especially in the triple-junction area [82,83], has been correlated with the emergence of good coercivity.

V. CONCLUSIONS AND OUTLOOK

Realistic modeling for Au-doped CeCu$_6$ and Co-doped CeCu$_5$ successfully describes the trends in magnetism involving the QCP on the basis of the localized $4f$ electrons. One of the archetypical HF materials family, CeCu$_6$, and its Au-doping-induced QCP can be described within a magnetic mechanism with the terms that can be naturally downfolded from the realistic electronic structure in the spirit of the Anderson model [26], without explicitly invoking valence fluctuations or introducing additional Heisenberg terms. We believe we have just put the characteristic energy scales of the target materials around the QCP under good numerical control in having succeeded in addressing the relative trends in magnetism around the QCP. We do not rule out other subtlety around the QCP that may come from other terms [23–25] that are not included in the present simulation framework. As long as the dominating energy scales are concerned, those other terms would not significantly alter the magnetism trend around the QCP.

Co doping in CeCu$_5$ drives the material on a wider scale on the chemical composition axis as compared to Au-doped CeCu$_6$. This is caused by magnetic fluctuations in the paramagnetic conduction band that is on the verge of ferromagnetism. For the $4f$-$3d$ intermetallic paramagnets in REPMs in general, small changes in the $3d$-metal concentration can drive the material around in the proximity of quantum criticality on the chemical composition space, rendering it easy to encounter critical regions in a microstructure with an appropriate spatial variance in the microchemistry.

Ce(Co, Cu)$_5$ represents one of the earliest and most typical materials families in REPMs [14,84]. The lattice structure of the materials family RT_5 including Ce(Co, Cu)$_5$ can be transformed into R_2T_{17} and RT_{12} [84] (R = rare earth and T = Fe group elements), and a local structure around the rare-earth sites in the champion magnet compound R_2Fe$_{14}$B (R = rare earth) resembles RT_5 as described in Sec. III A of Ref. [14]. With our results for Ce(Cu,Co)$_5$ in relation to Ce(Cu,Au)$_6$ concerning the QCP, it has been suggested that potentially various properties of derived compounds from the RT_5 archetypical series [85] residing in REPMs, especially physics in the crossover to the QCP, can be exploited for the possible intrinsic contribution to coercivity.

ACKNOWLEDGMENTS

M.M.'s work in Institute for Solid State Physics (ISSP), University of Tokyo, and High Energy Accelerator Research Organization (KEK) is supported by Toyota Motor Corporation. The author thanks C. E. Patrick for his careful reading of the manuscript. The author benefited from comments given by J. Otsuki and H. Sepehri-Amin. The author gratefully acknowledges helpful discussions with H. Shishido, T. Ueno, and K. Saito in related projects, crucial suggestions given by T. Akiya pointing to the particular materials family R(Cu, Co)$_5$ (R = rare earth), and an informative lecture given by K. Hono in the early stage of this project. The present work was partly supported by JSPS KAKENHI Grant No. 15K13525. Numerical computations were executed at the ISSP Supercomputer Center, University of Tokyo, and Numerical Materials Simulator in National Institute for Materials Science.

---

[1] J. Kondo, Resistance minimum in dilute magnetic alloys, Prog. Theor. Phys. **32**, 37 (1964).

[2] G. Hoffer and K. J. Strnat, Magnetocrystalline anisotropy of YCo$_5$ and Y$_2$Co$_{17}$, IEEE Trans. Mag. **2**, 487 (1966).

[3] E. A. Nesbitt, R. H. Willens, R. C. Sherwood, E. Buehler, and J. H. Wernick, New permanent magnet materials, Appl. Phys. Lett. **12**, 361 (1968).

[4] Y. Tawara and H. Senno, Cerium, cobalt, and copper alloy as a permanent magnet material, Jpn. J. Appl. Phys. **7**, 966 (1968).

[5] K. Andres, J. E. Graebner, and H. R. Ott, $4f$-Virtual-Bound-State Formation in CeAl$_3$ at Low Temperatures, Phys. Rev. Lett. **35**, 1779 (1975).

[6] S. Doniach, The Kondo lattice and weak antiferromagnetism, Physica B+C **91**, 231 (1977).

[7] F. Steglich, J. Aarts, C. D. Bredl, W. Lieke, D. Meschede, W. Franz, and H. Schäfer, Superconductivity in the Presence of Strong Pauli Paramagnetism: $CeCu_2Si_2$, Phys. Rev. Lett. **43**, 1892 (1979).

[8] M. Sagawa, S. Fujimura, N. Togawa, H. Yamamoto, and Y. Matsuura, New material for permanent magnets on a base of Nd and Fe, J. Appl. Phys. **55**, 2083 (1984).

[9] J. J. Croat, J. F. Herbst, R. W. Lee, and F. E. Pinkerton, Pr-Fe and Nd-Fe-based materials: A new class of high-performance permanent magnets, J. Appl. Phys. **55**, 2078 (1984).

[10] E. Bauer, E. Gratz, and C. Schmitzer, $CeCu_5$: Another Kondo lattice showing magnetic order, J. Magn. Magn. Mater. **63 & 64**, 37 (1987).

[11] For a review, see E. Bauer, Anomalous properties of Ce-Cu- and Yb-Cu-based compounds, Adv. Phys. **40**, 417 (1991).

[12] Y. Onuki, Y. Shimizu, and T. Komatsubara, Magnetic property of a new Kondo lattice intermetallic compound: $CeCu_6$, J. Phys. Soc. Jpn. **53**, 1210 (1984).

[13] G. R. Stewart, Z. Fisk, and M. S. Wire, New Ce heavy-fermion system: $CeCu_6$, Phys. Rev. B **30**, 482 (1984).

[14] For a review, see J. F. Herbst, $R_2Fe_{14}B$ materials: Intrinsic properties and technological aspects, Rev. Mod. Phys. **63**, 819 (1991).

[15] K. Hono and H. Sepehri-Amin, Strategy for high-coercivity Nd-Fe-B magnets, Scr. Mater. **67**, 530 (2012).

[16] K. Hono and H. Sepehri-Amin, Prospect for HRE-free high coercivity Nd-Fe-B permanent magnets, Scr. Mater. **151**, 6 (2018).

[17] For a review, see K. Ohashi, Present and future of Sm_2Co_{17} magnets, J. Jpn. Inst. Met. **76**, 96 (2012) (in Japanese except for abstract, key words, and figure captions).

[18] Y. Murakami, T. Tanigaki, T. T. Sasaki, Y. Takeno, H. S. Park, T. Matsuda, T. Ohkubo, K. Hono, and D. Shindo, Magnetism of ultrathin intergranular boundary regions in Nd-Fe-B permanent magnets, Acta Mater. **71**, 370 (2014).

[19] H. Sepehri-Amin, J. Thielsch, J. Fischbacher, T. Ohkubo, T. Schrefl, O. Gutfleisch, and K. Hono, Correlation of microchemistry of cell boundary phase and interface structure to the coercivity of $Sm(Co_{0.784}Fe_{0.100}Cu_{0.088}Zr_{0.028})_{7.19}$ sintered magnets, Act. Mater. **126**, 1 (2017).

[20] D. Girodin, C. H. Allibert, F. Givord, and R. Lemaire, Phase equilibria in the $CeCo_5$-$CeCu_5$ system and structural characterization of the $Ce(Co_{1-x}Cu_x)_5$ phases, J. Less Common Metals **110**, 149 (1985).

[21] H. v. Löhneysen, T. Pietrus, G. Portisch, H. G. Schlager, A. Schröder, M. Sieck, and T. Trappmann, Non-Fermi-Liquid Behavior in a Heavy-Fermion Alloy at a Magnetic Instability, Phys. Rev. Lett. **72**, 3262 (1994).

[22] A. Schröder, G. Aeppli, R. Coldea, M. Adams, O. Stockert, H. v. Löhneysen, E. Bucher, R. Ramazashvilis, and P. Coleman, Onset of antiferromagnetism in heavy-fermion metals, Nature (London) **407**, 351 (2000).

[23] Q. Si, S. Rabello, K. Ingersent, and J. L. Smith, Locally critical quantum phase transitions in strongly correlated metals, Nature (London) **413**, 804 (2001).

[24] P. Coleman, C. Pépin, Q. Si, and R. Ramazashvili, How do Fermi liquids get heavy and die, J. Phys.: Condens. Matter **13**, R723 (2001).

[25] For a recent review see, e.g., S. Kirchner, S. Paschen, Q. Chen, S. Wirth, D. Feng, J. D. Thompson, and Q. Si, Colloquium: Heavy-electron quantum criticality and single-particle spectroscopy, Rev. Mod. Phys. **92**, 011002 (2020).

[26] P. W. Anderson, Localized magnetic states in metals, Phys. Rev. **124**, 41 (1961).

[27] M. Matsumoto, M.-J. Han, J. Otsuki, and S. Y. Savrasov, First-Principles Simulations of Heavy Fermion Cerium Compounds Based on the Kondo Lattice, Phys. Rev. Lett. **103**, 096403 (2009).

[28] M. Matsumoto, M.-J. Han, J. Otsuki, and S. Y. Savrasov, Magnetic quantum critical point and dimensionality trend in cerium-based heavy-fermion compounds, Phys. Rev. B **82**, 180515(R) (2010).

[29] G. W. Scheerer, Z. Ren, S. Watanabe, G. Lapertot, D. Aoki, D. Jaccard, and K. Miyake, The dominant role of critical valence fluctuations on high T_c superconductivity in heavy fermions, npj Quantum Mater. **3**, 41 (2018).

[30] O. K. Andersen, Linear methods in band theory, Phys. Rev. B **12**, 3060 (1975).

[31] For the material-specific calculation of the hybridization function, we use the linear muffin-tin orbital method using the code described in S. Y. Savrasov, Linear-response theory and lattice dynamics: A muffin-tin-orbital approach, Phys. Rev. B **54**, 16470 (1996).

[32] J. Otsuki, H. Kusunose, P. Werner, and Y. Kuramoto, Continuous-time quantum Monte Carlo method for the Coqblin-Schrieffer model, J. Phys. Soc. Jpn. **76**, 114707 (2007).

[33] J. Otsuki, H. Kusunose, and Y. Kuramoto, The Kondo lattice model in infinite dimensions: I. Formalism, J. Phys. Soc. Jpn. **78**, 014702 (2009).

[34] J. Otsuki, H. Kusunose, and Y. Kuramoto, The Kondo lattice model in infinite dimensions: II. Static susceptibilities and phase diagram, J. Phys. Soc. Jpn. **78**, 034719 (2009).

[35] P. Hohenberg and W. Kohn, Inhomogeneous electron gas, Phys. Rev. **136**, B864 (1964).

[36] W. Kohn and L. J. Sham, Self-consistent equations including exchange and correlation effects, Phys. Rev. **140**, A1133 (1965).

[37] S. H. Vosko, L. Wilk, and M. Nusair, Accurate spin-dependent electron liquid correlation energies for local spin density calculations: A critical analysis, Can. J. Phys. **58**, 1200 (1980).

[38] For a review up to late 1990s, see V. I. Anisimov, A. I. Poteryaev, M. A. Korotin, A. O. Anokhin, and G. Kotliar, First-principles calculations of the electronic structure and spectra of strongly correlated systems: Dynamical mean-field theory, J. Phys.: Condens. Matter **9**, 7359 (1997).

[39] For a review up to mid 2000s, see G. Kotliar, S. Y. Savrasov, K. Haule, V. S. Oudovenko, O. Parcollet, and C. A. Marianetti, Electronic structure calculations with dynamical mean-field theory, Rev. Mod. Phys. **78**, 865 (2006).

[40] For a review including the fundamental aspects of downfolding to low-energy effective models from electronic structure calculations and the relative nature of the effective models defined with respect to the working energy window as introduced by the energy cutoff, see M. Imada and T. Miyake, J. Phys. Soc. Jpn. **79**, 112001 (2010).

[41] J. Hubbard, Proc. R. Soc. London Ser. A **276**, 238 (1963); **277**, 237 (1964); **281**, 401 (1964).

[42] J. R. Schrieffer and P. A. Wolff, Relation between the Anderson and Kondo Hamiltonians, Phys. Rev. **149**, 491 (1966).

[43] R. D. Cowan, *The Theory of Atomic Structure and Spectra* (University of California Press, Berkeley, CA, 1981).

[44] J. F. Herbst, R. E. Watson, and J. W. Wilkins, Relativistic calculations of $4f$ excitation energies in the rare-earth metals: Further results, Phys. Rev. B **17**, 3089 (1978), and references therein.

[45] Y. Baer and J. K. Lang, High-energy spectroscopy of f^{n+1} and f^{n-1} states in rare-earth metals, J. Appl. Phys. **50**, 7485 (1979).

[46] D. T. Cromer, A. C. Larson, and R. B. Roof, Jr., The crystal structure of $\mathrm{CeCu_6}$, Acta Crystallogr. **13**, 913 (1960).

[47] M. Ruck, G. Portisch, H. G. Schlager, M. Sieck, and H. v. Löhneysen, Structure and electrical resistivity of the heavy fermion compound $\mathrm{CeCu_5Au}$, Acta Crystallogr. B **49**, 936 (1993).

[48] H. Asano, M. Umino, Y. Õnuki, T. Komatsubara, F. Izumi, and N. Watanabe, Neutron diffraction study on the low-temperature monoclinic form of $\mathrm{CeCu_6}$, J. Phys. Soc. Jpn. **55**, 454 (1986).

[49] K. Grube, W. H. Fietz, U. Tutsch, O. Stockert, and H. v. Löhneysen, Suppression of the structural phase transition in $\mathrm{CeCu_6}$ by pressure and Au doping, Phys. Rev. B **60**, 11947 (1999).

[50] K. Uebayashi, K. Terao, and H. Hamada, First principle calculation for preferential site occupation of 3d transition-metal atoms in $\mathrm{YCo_5}$ and $\mathrm{YNi_5}$, J. Alloys Compd. **346**, 47 (2002).

[51] M. Matsumoto (unpublished).

[52] A. Georges, G. Kotliar, W. Krauth, and M. J. Rozenberg, Dynamical mean-field theory of strongly correlated fermion systems and the limit of infinite dimensions, Rev. Mod. Phys. **68**, 13 (1996).

[53] P. Werner, A. Comanac, L. de' Medici, M. Troyer, and A. J. Millis, Continuous-Time Solver for Quantum Impurity Models, Phys. Rev. Lett. **97**, 076405 (2006); P. Werner and A. J. Millis, Hybridization expansion impurity solver: General formulation and application to Kondo lattice and two-orbital models, Phys. Rev. B **74**, 155107 (2006).

[54] U. Witte, R. Schedler, O. Stockert, and M. Loewenhaupt, The investigation of the crystalline electric field of $\mathrm{CeCu_2}$ and $\mathrm{CeCu_6}$, J. Low Temp. Phys. **147**, 97 (2007).

[55] D. Gignoux, D. Schmitt, E. Bauer, and A. P. Murani, Inelastic neutron scattering in some hexagonal cerium compounds, J. Magn. Magn. Mater. **88**, 63 (1990).

[56] For a review, see R. Settai, T. Takeuchi, and Y. Onuki, Recent advances in Ce-based heavy-fermion superconductivity and Fermi surface properties, J. Phys. Soc. Jpn. **76**, 051003 (2007).

[57] B. Mühlschlegel, Relation between the Anderson and Kondo Hamiltonians for the case of degenerate impurity orbitals, Z. Phys. **208**, 94 (1968).

[58] M. Matsumoto, Navigating the trends in the proximity to magnetic quantum critical point and superconductivity for Ce-based heavy-fermion compounds, J. Phys. Soc. Jpn. **88**, 114705 (2019).

[59] F. Gebhard, *The Mott Metal-Insulator Transition*, Springer Tracts in Modern Physics Vol. 137 (Springer-Verlag, Berlin, 1997).

[60] K. Yosida, Magnetic properties of Cu-Mn alloys, Phys. Rev. **106**, 893 (1957).

[61] M. A. Ruderman and C. Kittel, Indirect exchange coupling of nuclear magnetic moments by conduction electrons, Phys. Rev. **96**, 99 (1954)

[62] T. Kasuya, A theory of metallic ferro- and antiferromagnetism on Zener's model, Prog. Theor. Phys. **16**, 45 (1956).

[63] I. A. Campbell, Indirect exchange for rare earths in metals, J. Phys. F: Met. Phys. **2**, L47 (1972).

[64] In our related work, M. Matsumoto, H. Akai, Y. Harashima, S. Doi, and T. Miyake, Relevance of $4f$-$3d$ exchange to finite-temperature magnetism of rare-earth permanent magnets: An *ab-initio*-based spin model approach for $\mathrm{NdFe_{12}N}$, J. Appl. Phys. **119**, 213901 (2016), a manual rescaling of J_{RT} was attempted on top of a set of *ab initio* numbers for $3d$-$5d$ exchange couplings that are calculated following Ref. [65].

[65] A. I. Liechtenstein, M. I. Katsnelson, V. P. Antropov, and V. A. Gubanov, Local spin density functional approach to the theory of exchange interactions in ferromagnetic metals and alloys, J. Magn. Magn. Mater. **67**, 65 (1987).

[66] Y. Toga, M. Matsumoto, S. Miyashita, H. Akai, S. Doi, T. Miyake, and A. Sakuma, Monte Carlo analysis for finite-temperature magnetism of $\mathrm{Nd_2Fe_{14}B}$ permanent magnet, Phys. Rev. B **94**, 174433 (2016).

[67] C. Wetli, S. Pal, J. Kroha, K. Kliemt, C. Krellner, O. Stockert, H. v. Löhneysen, and M. Fiebig, Time-resolved collapse and revival of the Kondo state near a quantum phase transition, Nat. Phys. **14**, 1103 (2018).

[68] S. Pal, C. Wetli, F. Zamani, O. Stockert, H. v. Löhneysen, M. Fiebig, and J. Kroha, Fermi Volume Evolution and Crystal-Field Excitations in Heavy-Fermion Compounds Probed by Time-Domain Terahertz Spectroscopy, Phys. Rev. Lett. **122**, 096401 (2019).

[69] Y. Kuramoto, Self-consistent perturbation theory for dynamics of valence fluctuations I. Single-site theory, Z. Phys. B **53**, 37 (1983).

[70] For a review see, e.g., N. E. Bickers, Review of techniques in the large-N expansion for dilute magnetic alloys, Rev. Mod. Phys. **59**, 845 (1987).

[71] For a review see, e.g., M. Jarrel and J. E. Gubernatis, Phys. Rep. **269**, 133 (1996).

[72] For recent developments see, e.g., J. Otsuki, M. Ohzeki, H. Shinaoka, and K. Yoshimi, Sparse modeling approach to analytical continuation of imaginary-time quantum Monte Carlo data, Phys. Rev. E **95**, 061302(R) (2017); H. Shinaoka, J. Otsuki, M. Ohzeki, and K. Yoshimi, Compressing Green's function using intermediate representation between imaginary-time and real-frequency domains, Phys. Rev. B **96**, 035147 (2017).

[73] T. Schäfer, A. A. Katanin, M. Kitatani, A. Toschi, and K. Held, Quantum Criticality in the Two-Dimensional Periodic Anderson Model, Phys. Rev. Lett. **122**, 227201 (2019).

[74] E. Lectard, C. H. Allibert, and R. Ballou, Saturation magnetization and anisotropy fields in the $\mathrm{Sm(Co_{1-x}Cu_x)_5}$ phases, J. Appl. Phys. **75**, 6277 (1994).

[75] T. Endstra, G. J. Nieuwenhuys, and J. A. Mydosh, Hybridization model for the magnetic-ordering behavior of uranium- and cerium-based 1:2:2 intermetallic compounds, Phys. Rev. B **48**, 9595 (1993).

[76] S. V. Vonsovskii, Zh. Eksp. Teor. Fiz. **16**, 981 (1946) [Sov. Phys. JETP **10**, 468 (1946)].

[77] C. Zener, Interaction between the d shells in the transition metals, Phys. Rev. **81**, 440 (1951).

[78] N. E. Sluchanko, On the limits of application of Anderson and Kondo models in physics of strongly correlated electron

systems, Low Temp. Phys. **41**, 544 (2015), and references therein.

[79] For a review on recent developments see, e.g., G. Carleo, I. Cirac, K. Cranmer, L. Daudet, M. Schuld, N. Tishby, L. Vogt-Maranto, and L. Zdeborová, Machine learning and the physical sciences, Rev. Mod. Phys. **91**, 045002 (2019).

[80] J. Otsuki, H. Kusunose, and Y. Kuramoto, Evolution of a Large Fermi Surface in the Kondo Lattice, Phys. Rev. Lett. **102**, 017202 (2009).

[81] C. E. Patrick, M. Matsumoto, and J. B. Staunton, First-principles calculations of the magnetocrystalline anisotropy of the prototype 2:17 cell boundary phase $\mathrm{Y(Co_{1-x-y}Fe_xCu_y)_5}$, J. Magn. Magn. Mater. **477**, 147 (2019).

[82] Y. Zhang, W. Tang, G. C. Hadjipanayis, C. Chen, C. Nelson, and K. Krishnan, IEEE Trans. Magn. **37**, 2525 (2001).

[83] X. Y. Xiong, T. Ohkubo, T. Koyama, K. Ohashi, Y. Tawara, and K. Hono, The microstructure of sintered $\mathrm{Sm(Co_{0.72}Fe_{0.20}Cu_{0.055}Zr_{0.025})_{7.5}}$ permanent magnet studied by atom probe, Acta Mater. **52**, 737 (2004).

[84] H. S. Li and J. M. D. Coey, Magnetic properties of ternary rare-earth transition-metal compounds, in *Handbook of Magnetic Materials*, edited by K. H. J. Buschow (Elsevier, Amsterdam, 1991), Vol. 6, Chap. 1, pp. 1–83.

[85] For a recent thorough investigation from first principles over the series $R\mathrm{Co}_5$, see, e.g., C. E. Patrick and J. B. Staunton, Temperature-dependent magnetocrystalline anisotropy of rare earth/transition metal permanent magnets from first principles: The light $R\mathrm{Co}_5$ (R=Y, La-Gd) intermetallics, Phys. Rev. Mater. **3**, 101401(R) (2019).